

Diagnostics for specific PAHs in the far-IR: searching neutral naphthalene and anthracene in the Red Rectangle

G. Mulas^{1,2}, G. Mallocci², C. Joblin², and D. Toublanc²

¹ INAF – Osservatorio Astronomico di Cagliari – Astrochemistry Group, Strada 54, Loc. Poggio dei Pini, I–09012 Capoterra (CA), Italy — e-mail: gmulas@ca.astro.it

² Centre d'Etude Spatiale des Rayonnements, CNRS et Université Paul Sabatier–Toulouse 3, Observatoire Midi-Pyrénées, 9 Avenue du Colonel Roche, 31028 Toulouse Cedex 04, France — e-mail: [giuliano.malloci; christine.joblin; dominique.toublanc]@cesr.fr

Received ?; accepted ?

Abstract. *Context.* In the framework of the interstellar polycyclic aromatic hydrocarbons (PAHs) hypothesis, far-IR skeletal bands are expected to be a fingerprint of single species in this class.

Aims. We address the question of detectability of low energy PAH vibrational bands, with respect to spectral contrast and intensity ratio with “classical” Aromatic Infrared Bands (AIBs).

Methods. We extend our established Monte-Carlo model of the photophysics of specific PAHs in astronomical environments, to include rotational and anharmonic band structure. The required molecular parameters were calculated in the framework of the Density Functional Theory.

Results. We calculate the detailed spectral profiles of three low-energy vibrational bands of neutral naphthalene, and four low-energy vibrational bands of neutral anthracene. They are used to establish detectability constraints based on intensity ratios with “classical” AIBs. A general procedure is suggested to select promising diagnostics, and tested on available Infrared Space Observatory data for the Red Rectangle nebula.

Conclusions. The search for single, specific PAHs in the far-IR is a challenging, but promising task, especially in view of the forthcoming launch of the Herschel Space Observatory.

Key words. Astrochemistry — Line: identification — Molecular processes — ISM: individual objects: Red Rectangle — ISM: lines and bands — ISM: molecules

1. Introduction

The presence of polycyclic aromatic hydrocarbons (PAHs) in the interstellar medium (ISM) was proposed by Léger & Puget (1984) and Allamandola et al. (1985), to account for the so-called “Aromatic Infrared Bands” (AIBs), a set of emission bands observed near 3.3, 6.2, 7.7, 8.6, 11.3 and 12.7 μm , in many dusty environments excited by UV photons (Léger et al. 1989; Allamandola et al. 1989). Such “classical” AIBs do not permit an unambiguous identification of any single PAH, since they just probe specific chemical bonds and not its overall structure. Indeed, despite the impressive amount of work devoted to this subject over the years, no *definitive* spectral identification of any *specific* individual member in this class exists to date. On the other hand, every single such PAH ought to show a unique spectral fingerprint in the far-IR spectral region, which contains the low-frequency vibrational modes associated with collective oscillations of the whole skeletal structure of the molecule (Zhang et al. 1996; Langhoff 1996; Salama 1999; Joblin et al. 2002; Mulas et al. 2003, 2006a,b).

In Mulas et al. (2006b) we presented and validated a procedure to model in a systematic way the photophysics of PAHs in photon dominated regions. In that work, we computed the complete far-IR emission spectrum of a sample of 20 molecules and their cations in three radiation fields, covering some typical astronomical environments in which AIBs are observed. We concluded that the main problem for the detection and identification of such bands is likely to be spectral confusion and poor contrast against a strong background continuum: perpendicular bands, which are expected to display sharp Q branches, are much favoured with respect to shallower parallel bands.

Our approach can also model molecular rotation and thus obtain the expected band rotational envelopes of both far-IR emission bands (Joblin et al. 2002) and visible absorption bands (Mallocci et al. 2003). It can also estimate the contributions of fundamental and hot bands, with their distribution of anharmonic shifts, which affect the expected band profile. This makes modelling much heavier: if J_{\max} is the maximum angular momentum which is significantly populated, $J_{\max}(J_{\max} + 1)$ is the number of rotational levels which must be traced, during the simulation, for each vibrational mode. Since for the

molecules considered J_{\max} is a few hundred (Rouan et al. 1997; Mulas 1998), this makes the simulation $J_{\max} (J_{\max} + 1) \sim 10^5$ times more demanding from a computational point of view. Furthermore, it requires the knowledge of the effective rotational constants as a function of vibrational state and of the anharmonic correction for hot bands.

To elucidate the role of spectral shape on band detectability, we present here, as a test case, a detailed calculation for three low-frequency bands of the simplest PAH, namely neutral naphthalene ($C_{10}H_8$), and for four low-frequency bands of the next larger PAH in the group of oligoacenes, i. e. neutral anthracene. ($C_{14}H_{10}$). In particular, for naphthalene we selected the lowest energy a-type, b-type and c-type transition, whose fundamental wavelengths are calculated to be respectively at 15.82, 27.74 and 58.56 μm ; for anthracene, we selected the lowest energy a-type (43.68 μm) and c-type (21.26, 26.35 and 110.23 μm) bands.

In the following Sect. 2 we present our modelling approach. Results are then presented in Sect. 3 and discussed in Sect. 4.

2. Modelling approach

Our Monte-Carlo modelling procedure is described in detail elsewhere (Mulas 1998; Joblin et al. 2002; Malloci et al. 2003; Mulas et al. 2003, 2006a,b), as well as the basic molecular parameters it requires. We here use exactly the same photo-absorption cross-sections and vibrational analyses of neutral naphthalene and neutral anthracene as in Mulas et al. (2006b), where their applicability and accuracy is discussed in detail. Since this is a proof-of-concept work, we restricted ourselves to one single well-known environment, i. e. the Red Rectangle (RR) halo, using the same radiation field (RF) previously adopted for it in Mulas et al. (2006a), derived from the observational work of Vlijh et al. (2005).

We here additionally studied in detail the distribution of anharmonic shifts arising from the superposition of a large number of hot bands on top of the fundamental band, in the stochastic process of PAH relaxation via IR emission. Moreover, we also calculated detailed rotational profiles obtained from statistical equilibrium.

To do this we needed the previously unavailable anharmonic correction to vibrational terms and rotational constants, and the Coriolis vibration-rotation coupling, which we computed using the GAUSSIAN03 quantum chemistry package (Frisch et al. 2003). This implements the Van Vleck perturbative approach to the above problem (e. g. Clabo et al. 1988), which we applied in the framework of the Density Functional Theory, with the exchange-correlation functional B3LYP (Becke 1993; Stephens et al. 1994) and the 4-31G gaussian basis set (Frish et al. 1984). While basis set convergence is not achieved yet at this level of theory, it is good enough to yield sensible results. Indeed, benchmark calculations showed that smaller basis sets are required to obtain good perturbative corrections than are needed for equilibrium geometry properties and harmonic vibrational analyses (Barone 2004, 2005).

The anharmonic vibrational analysis yields the second-order anharmonic corrections to the vibrational energy

levels, which are represented, in wavenumbers, by the formula (see e. g. Barone 2005, and references therein):

$$E_{\text{vib}}(n_1, \dots, n_N) = \chi_0 + \sum_i \left(n_i + \frac{1}{2} \right) \bar{\omega}_i + \sum_{i,j \geq i} \chi_{ij} \left(n_i + \frac{1}{2} \right) \left(n_j + \frac{1}{2} \right),$$

where χ_0 and χ_{ij} are the vibrational anharmonic constants as defined in Barone & Minichino (1995) with the corrections reported in Barone (2004). The values of χ_{ij} which we obtained are listed in Tables A.1 and A.3 in the Appendix for the specific bands we considered here.

Accidental near degeneracies, when they occur, lead to additional corrections (i. e. Fermi and Darling-Dennison resonances), which are not systematic and must thus be evaluated, if relevant, on a case by case basis. For the three specific benchmark bands which we modelled here for neutral naphthalene, the levels from which emission is estimated to occur significantly (fundamental and first few hot bands) are unperturbed by such resonances. For bands for which they do occur, in the case of neutral naphthalene and anthracene they are smaller than anharmonic corrections anyway, so that the qualitative conclusions we may draw from our test cases remain valid.

To leading order, selection rules are the same as in the harmonic approximation, i. e. they connect levels in which a single IR-active mode changes by one quantum. The energy difference

$$\Delta E_k(n_1, \dots, n_N) = E_{\text{vib}}(\dots, n_k + 1, \dots) - E_{\text{vib}}(\dots, n_k, \dots)$$

for a transition in which only the k^{th} quantum number changes as $n_k + 1 \rightarrow n_k$ is hence given by

$$\Delta E_k(n_1, \dots, n_N) = \bar{\omega}_k + 2\chi_{kk}(n_k + 1) + \sum_{i \neq k} \chi_{ik} \left(n_i + \frac{1}{2} \right),$$

which may be rewritten as

$$\Delta E_k(n_1, \dots, n_N) = \Delta E_k(0, \dots, 0) + 2\chi_{kk}n_k + \sum_{i \neq k} \chi_{ik}n_i.$$

This equation shows that anharmonicity produces a shift in the hot bands, with respect to the fundamental, which is proportional to the vibrational quantum numbers in the lower energy state involved in the transition. Since IR emission by PAHs results from a vibrational cascade, a given band will result in the superposition of the fundamental plus a possibly large number of hot bands, their contributions depending on the detailed statistics of the process. This in turn results in a distribution of anharmonic shifts, which convolves the pure (non-thermal) rotational envelope of the band. Both effects are sampled by our Monte-Carlo procedure.

On top of this, each single transition, due to higher order perturbative effects, turns into the superposition of transitions including a distribution of nearby states. This produces a lorentzian envelope, i. e. lifetime broadening, with a width which roughly scales with the density of vibrational states at the energy at which the transition occurs. Since bands in the low-energy modes are emitted near the end of the vibrational cascades (see Figs. 1 and 2), below or slightly above the decoupling energy (we assumed $E_{\text{dec}} \simeq 0.32$ eV for neutral

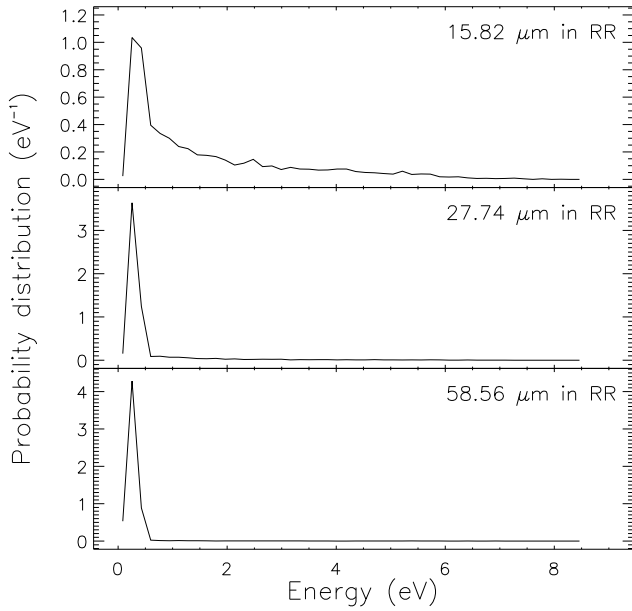


Fig. 1. Probability distribution of the excitation energies at which photons are emitted in the three bands considered of neutral naphthalene in the RR halo.

naphthalene and 0.21 eV for neutral anthracene, Mulas et al. 2006b), we neglect lifetime broadening in our present simulation. Specifically, two of the three bands we modelled for naphthalene and three of the four for anthracene are emitted virtually *only* below E_{dec} ; only the highest energy band we considered for each molecule is emitted in a non negligible fraction at excitation energies above E_{dec} . Moreover, comparison with experimental spectra of gas-phase naphthalene at room temperature show a rather good correspondence of the band near $\sim 12.8 \mu\text{m}$ with a theoretical spectrum we calculated under these same assumptions (Pirali et al. 2006).

As to the change of the effective rotational constants as a function of vibrational state, to leading order they have a linear dependence on vibrational quantum numbers, i. e.

$$A_{\text{eff}}(n_1, \dots, n_N) = A_{\text{eff}}(0, \dots, 0) - \sum_i a_i n_i$$

and equivalent relations for B_{eff} and C_{eff} . The a_i , b_i and c_i constants (the so-called α matrix), which include three leading contributions from harmonic, anharmonic and Coriolis terms in the molecular Hamiltonian, are almost all very small for naphthalene and anthracene, producing changes in the range of a few parts in a thousand in the effective rotational constants. We report them in Tables A.2 and A.4 in the Appendix.

Only in two cases, for naphthalene, the accidental near resonance of the two vibrational modes respectively at 15.82 and $15.90 \mu\text{m}$ and at 19.49 and $19.54 \mu\text{m}$ produces large Coriolis coupling terms between them, resulting in a $\sim 4\%$ change in the affected rotational constant as a function of the number of quanta in that vibrational state. In the case of anthracene, the largest change in the rotational constants is less than 0.9%,

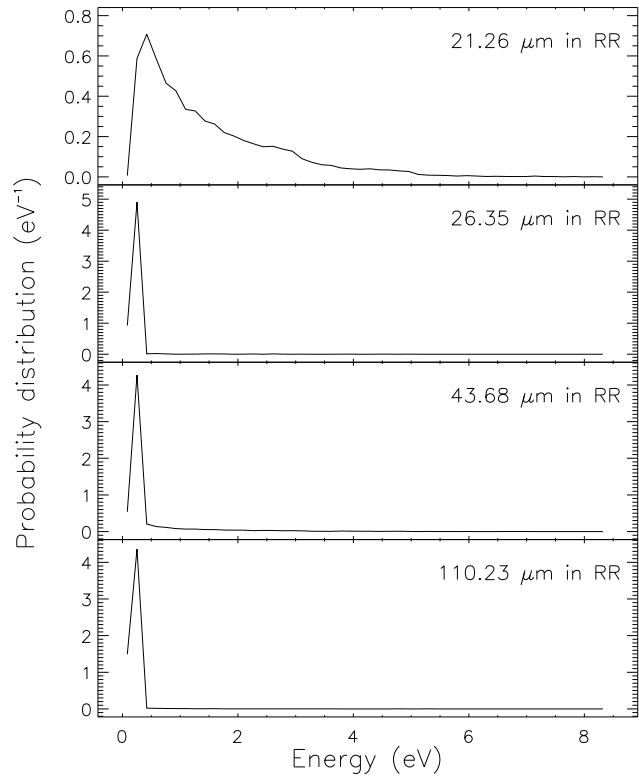


Fig. 2. Same as Fig. 1 for the four bands considered of neutral anthracene.

again due to an accidental near resonance between the modes at 25.45 and $26.62 \mu\text{m}$.

3. Results

3.1. Calculated band profiles

The three bands of neutral naphthalene for which we modelled the detailed rovibrational and anharmonic structure are one of each type, i. e. an a-type, a b-type and a c-type band respectively. They are two in-plane and one out-of-plane (the latter being the so-called “butterfly” or “flopping”) bending modes, and each of them is the lowest frequency transition of its type. For neutral anthracene we modelled the four lowest frequency bands, which are, in order of decreasing energy, two c-type, one a-type and another c-type.

Since the lowest energy butterfly mode of both molecules falls in the spectral range of the Long Wavelength Spectrograph (LWS) on board ISO, we convolved their synthetic spectra with the average resolving power of LWS with ($R \approx 8250$) and without ($R \approx 175$) the Fabry–Perot filter, assuming a velocity dispersion $\lesssim 5 \text{ km s}^{-1}$. Similarly, since all other bands fall in the spectral range covered by the Short Wavelength Spectrograph (SWS) of ISO, we convolved their synthetic spectra with the resolving power of SWS with ($R \approx 30000$) and without ($R \approx 1500$) the Fabry–Perot filter, with the same velocity dispersion. For

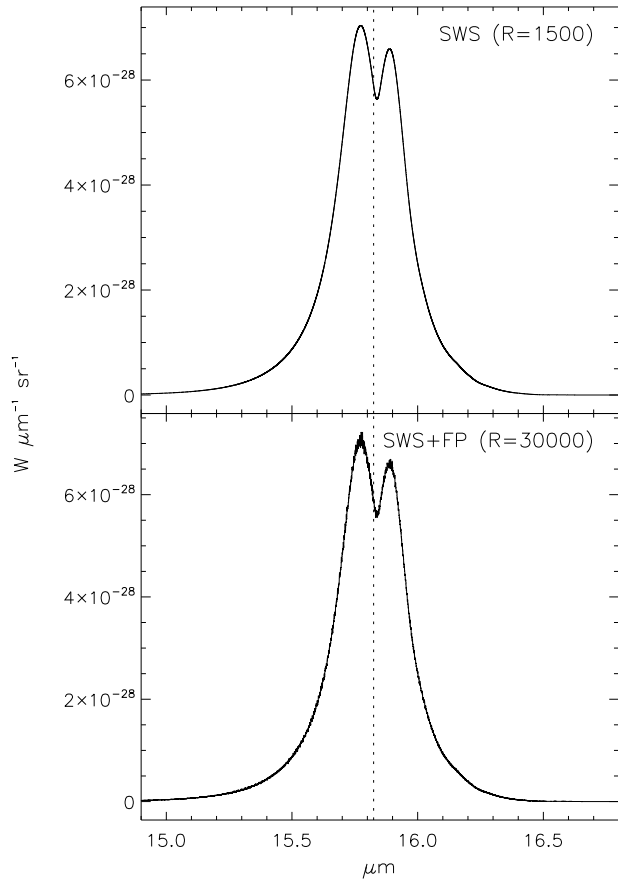


Fig. 3. Detailed rotational structure of the band at $15.82\text{ }\mu\text{m}$ of neutral naphthalene in the RR halo. Strong Cariolis coupling with the IR–inactive band at $15.90\text{ }\mu\text{m}$ causes one of the rotational constants to differ by $\sim 4\%$ between the upper and lower vibrational states involved in the transition, producing a blue shaded rotational profile. The superposition of hot bands, which has a red–shaded envelope, acts in the opposite direction, so that the overall profile including both effects is almost symmetric. The two panels show the band as would be seen with ISO–SWS with and without the Fabry–Perot filter. The vertical dotted line marks the position of the origin of the fundamental band.

details on SWS and LWS, see their manuals on the official ISO web page¹. The resulting spectra are shown in figures 3 to 9.

There is clearly a qualitative difference between perpendicular and parallel bands, i. e. the presence of a central Q branch containing about 20% of the total flux in the band. Such difference is very apparent in the bands at $58.56\text{ }\mu\text{m}$ of naphthalene and at $26.35\text{ }\mu\text{m}$ of anthracene: in these cases, the rotational constants are very nearly the same in the two vibrational modes involved in the transition, which makes the resulting Q branches extremely sharp, with a full width at half maximum (FWHM) of the order of $\sim 0.15\text{ cm}^{-1}$. Moreover, in the absence

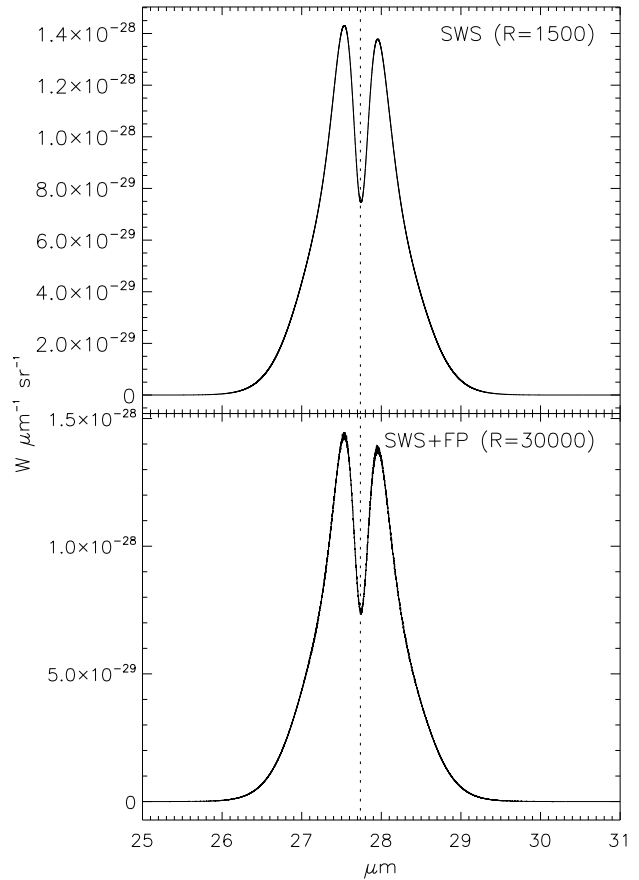


Fig. 4. Same as Fig. 3 for the naphthalene band at $27.74\text{ }\mu\text{m}$. The rotational constants are almost unchanged in the vibrational transition, resulting in a very symmetric rotational envelope, the asymmetry being mainly due to the superposition of slightly displaced sovratones of the band.

of shading², neither the P nor the R branch is inverted, and the Q branch sits in the gap between them, with little contamination. The superposition of the fundamental and hot bands produces a well defined pattern of anharmonic shifts, clearly visible in the zoomed inset in the lower panel of Figs. 5, 7 and 9. With the low resolution mode of LWS, the fundamental and hot bands merge in an unique, unresolved, red–shaded Q branch, with a FWHM corresponding to the resolving power of the instrument. The P and R branches have a FWHM of the order of $\sim 8\text{ cm}^{-1}$.

In the band at $21.26\text{ }\mu\text{m}$ of anthracene, instead, the larger difference in rotational constants between the states involved in the transition and the pattern of anharmonic shifts of the hot bands effectively masks the central Q branch, which is just barely visible in the high resolution panel of Fig. 6.

² A difference in the rotational constants between the upper and lower states involved in a transition leads to the inversion of some branches, with the consequent formation of band heads, and results in an overall asymmetry in the rotational profile. A band is then commonly said to be *red–shaded* when it has a more extended tail on the red side, *blue–shaded* in the opposite case (Herzberg 1991a,b)

¹ <http://www.iso.vilspa.esa.es>

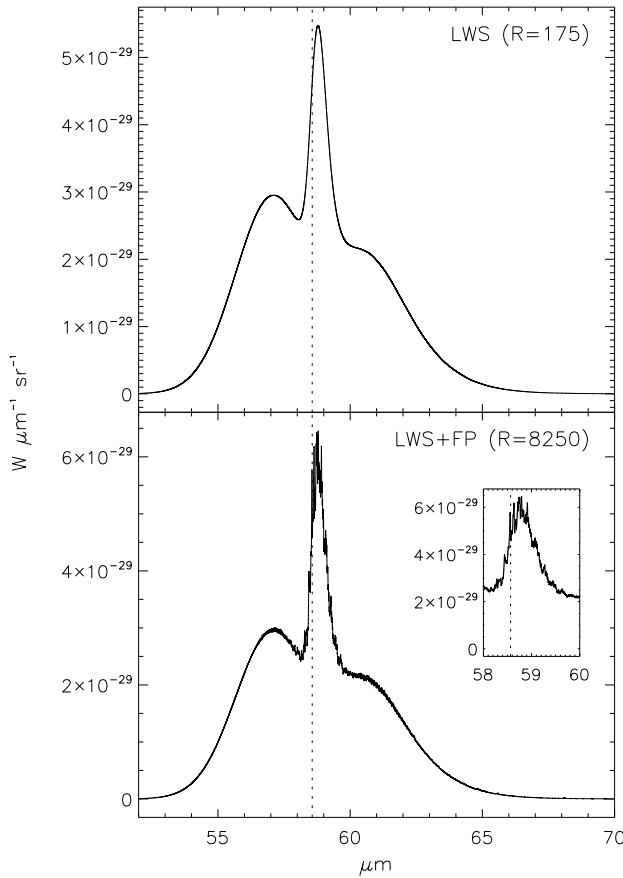


Fig. 5. Same as Fig. 3 for the naphthalene band at 58.56 μm . The rotational constants are almost unchanged in the vibrational transition, resulting in a very symmetric rotational envelope, with a Q branch standing out very clearly. The two panels show the band as would be seen with ISO-LWS with and without the Fabry–Perot filter. In the lower panel, the higher resolving power allows the resolution, in the Q branch, of the separate contributions of different hot bands, with slightly different anharmonic shifts (zoomed inset).

The parallel bands of naphthalene are resolved in only two well-defined features, which in the b-type one at 27.74 μm include a split Q branch (Herzberg 1991b). The width of these partially resolved features is approximately $\sim 6 \text{ cm}^{-1}$. As to the parallel band of anthracene at 43.68 μm , relatively strong red shading and anharmonicity combine to produce a single, unresolved, asymmetric feature with an approximate FWHM of $\sim 6 \text{ cm}^{-1}$.

These differences in band shapes, which depend on the interplay of many molecular parameters, have direct consequences on their detectability.

3.2. Comparison with observations

We here examine in detail the case of the RR nebula, which is one of the reference targets for the observation of AIBs and thus a prime candidate for the identification of specific PAHs

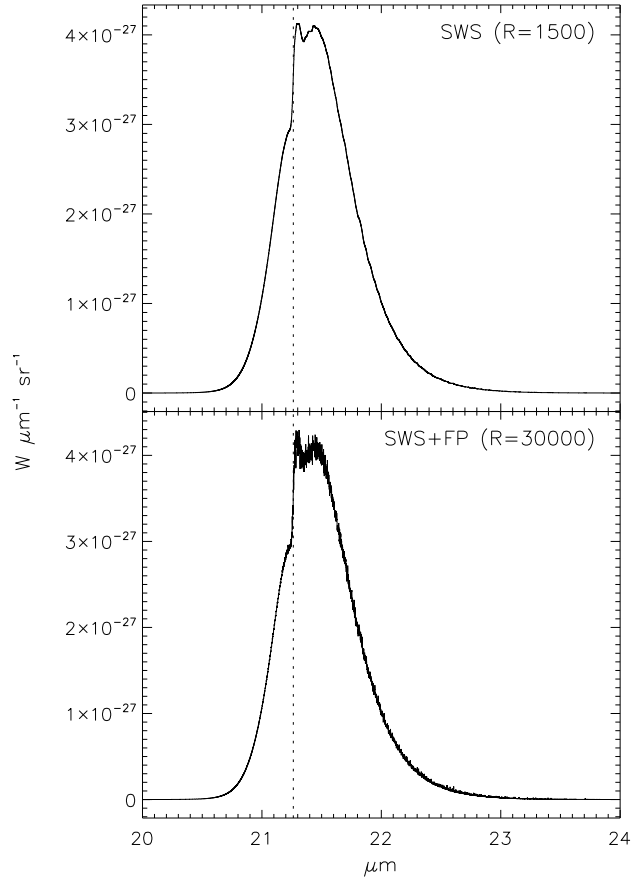


Fig. 6. Detailed rotational structure of the band at 21.26 μm of neutral anthracene in the RR halo. The rotational constants are almost unchanged in the vibrational transition, resulting in a very symmetric rotational envelope, with a visible Q branch whose width is due to the superposition of hot bands with different anharmonic shifts. The two panels show the band as would be seen with ISO-SWS with and without the Fabry–Perot filter. The vertical dotted lines marks the position of the origin of the fundamental band.

in space. ISO data for this object are available in the online archive. Under optically thin conditions, the observed spectrum of a given band produced by a given PAH, for instance neutral naphthalene, is

$$\frac{dF}{d\lambda} = \frac{dF_{\text{cont}}}{d\lambda} + \int dr d\Omega n_{\text{naph.}} \frac{d\mathcal{P}}{d\lambda}, \quad (1)$$

where $\frac{dF_{\text{cont}}}{d\lambda}$ is the underlying continuum spectrum, $\frac{d\mathcal{P}}{d\lambda}$ is the power isotropically emitted in the band by one molecule for the assumed RF, $n_{\text{naph.}}$ is its number density and the double integral is along the line of sight and over the solid angle observed. As explained in detail in Mulas et al. (2006b), the IR spectrum emitted by a species in a given regime scales linearly with the intensity of the RF. Since extinction in the RR halo is negligible (Vijh et al. 2005), the RF will change only due to dilution with

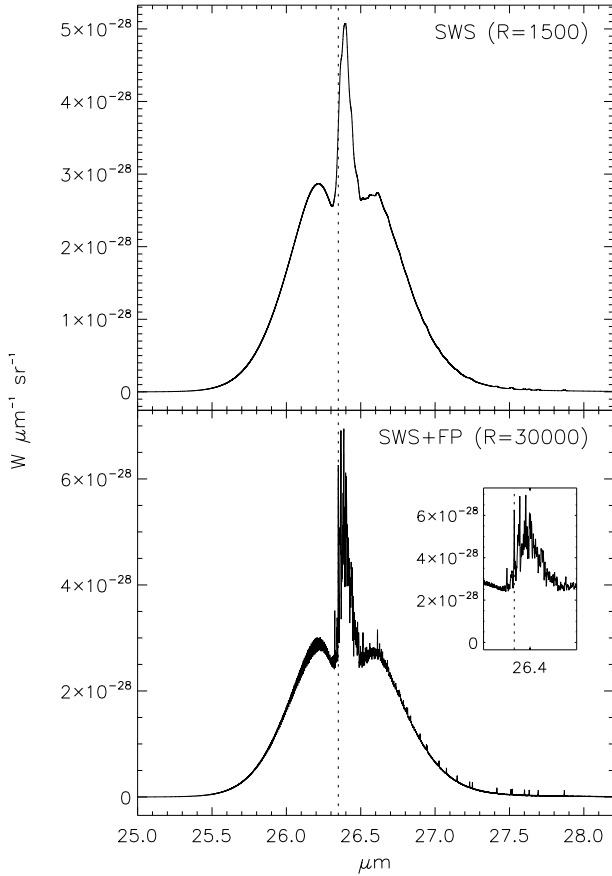


Fig. 7. Same as Fig. 6 for the anthracene band at $26.35\text{ }\mu\text{m}$. The rotational constants are almost unchanged in the vibrational transition, resulting in a very symmetric rotational envelope, with a sharp Q branch standing clearly out in the middle. In the lower panel, the higher resolving power allows the resolution, in the Q branch, of the separate contributions of different hot bands, with slightly different anharmonic shifts (zoomed inset).

the position in the nebula and such scaling relations are valid in this case. Hence, we can factor $\frac{d\mathcal{P}}{d\lambda}$ as

$$\frac{d\mathcal{P}}{d\lambda} = \frac{d\mathcal{P}_{\text{ref}}}{d\lambda} \Lambda(r, \Omega),$$

where $\Lambda(r, \Omega)$ is an adimensional scaling factor, independent of λ , which takes into account the variation of RF intensity with position in the source and $\frac{d\mathcal{P}_{\text{ref}}}{d\lambda}$ is independent of r and Ω . We may thus rewrite Eq. (1) as

$$\begin{aligned} \frac{dF}{d\lambda} &= \frac{dF_{\text{cont}}}{d\lambda} + \frac{d\mathcal{P}_{\text{ref}}}{d\lambda} \int dr d\Omega n_{\text{naph.}} \Lambda(r, \Omega) \\ &= \frac{dF_{\text{cont}}}{d\lambda} + \frac{d\mathcal{P}_{\text{ref}}}{d\lambda} \Upsilon_{\text{naph.}}, \end{aligned} \quad (2)$$

where $\Upsilon_{\text{naph.}}$, defined above, has the dimensions of a column density times a solid angle and is independent of λ . Classical AIBs are commonly considered as typical tracers of PAHs.

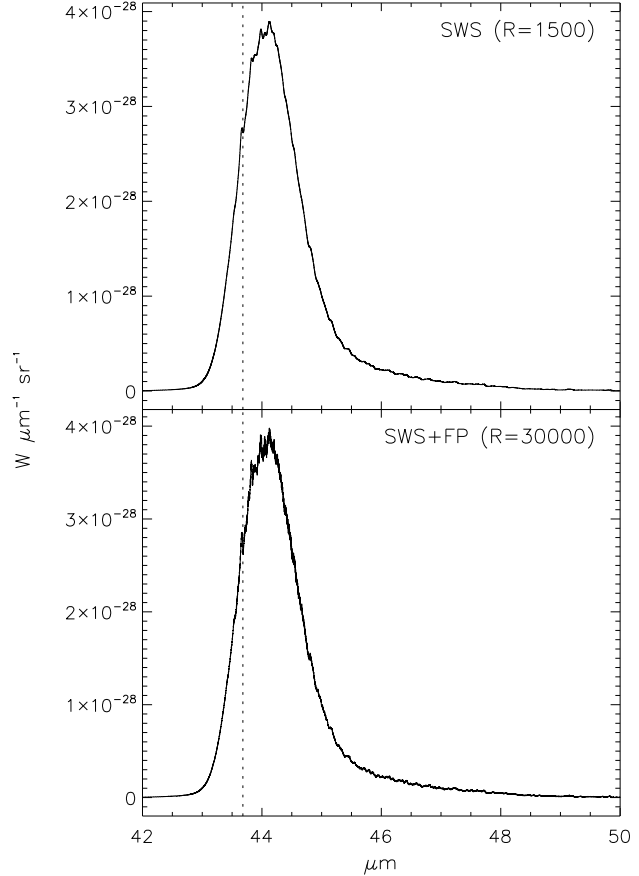


Fig. 8. Same as Fig. 6 for the anthracene band at $43.68\text{ }\mu\text{m}$. The relatively large change in the rotational constants in the vibrational transition results in a visibly red-shaded band.

Using Eq. (2) and integrating over one AIB, we obtain

$$\begin{aligned} \int_{\text{AIB}} d\lambda \left(\frac{dF}{d\lambda} - \frac{dF_{\text{cont}}}{d\lambda} \right) &= \Upsilon_{\text{naph.}} \int_{\text{AIB}} d\lambda \frac{d\mathcal{P}_{\text{ref}}}{d\lambda} \\ &= \Upsilon_{\text{naph.}} \mathcal{P}_{\text{AIB}} = \eta_{\text{AIB}} F_{\text{AIB}}, \end{aligned}$$

where η_{AIB} is the fraction of the flux in the AIB produced by the given molecule and \mathcal{P}_{AIB} is the result of our model for the reference RF and the chosen band. Solving the above equation for $\Upsilon_{\text{naph.}}$, we get

$$\Upsilon_{\text{naph.}} = \eta_{\text{AIB}} \frac{F_{\text{AIB}}}{\mathcal{P}_{\text{AIB}}}. \quad (3)$$

Let's now focus on another IR band of the same specific PAH. To be detectable, it must stand above the continuum by more than the noise level, i. e., for a 2σ detection:

$$\frac{\frac{dF_{\text{peak}}}{d\lambda} - \frac{dF_{\text{cont}}}{d\lambda}}{\frac{dF_{\text{cont}}}{d\lambda}} \gtrsim \frac{2}{S},$$

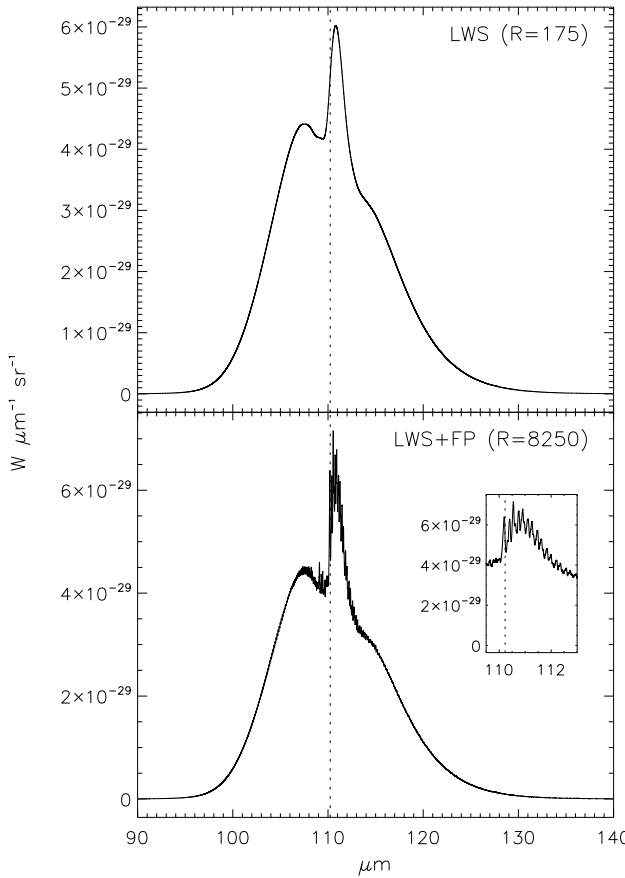


Fig. 9. Same as Fig. 6 for the anthracene band at 110.23 μm . The change in rotational constants, combined with the superposition of hot bands, produces an asymmetric profile, in the middle of which a sharp Q branch clearly stands out. In the lower panel, the higher resolving power allows the resolution, in the Q branch, of the separate contributions of different hot bands, with slightly different anharmonic shifts (zoomed inset).

S being the signal to noise ratio, from which follows, using Eq. (2) and then Eq. (3),

$$\frac{\left(\frac{d\mathcal{P}_{\text{ref}}}{d\lambda}\right)_{\text{peak}} \Upsilon_{\text{naph.}}}{\frac{dF_{\text{cont}}}{d\lambda}} = \frac{\left(\frac{d\mathcal{P}_{\text{ref}}}{d\lambda}\right)_{\text{peak}} \eta_{\text{AIB}} \frac{F_{\text{AIB}}}{\mathcal{P}_{\text{AIB}}}}{\frac{dF_{\text{cont}}}{d\lambda}} \gtrsim \frac{2}{S}.$$

In the equation above, we implicitly assumed both this latter band and the reference AIB are integrated over the same aperture on the sky. For ISO observations of the RR, this is a good assumption since RR is completely contained both in the SWS and in the LWS entrance apertures (Bregman et al. 1993; Men'shchikov et al. 2002). Solving for η_{AIB} , we finally obtain that the band will be detected only if

$$\eta_{\text{AIB}} \gtrsim \frac{2}{S} \frac{\frac{dF_{\text{cont}}}{d\lambda}}{\left(\frac{d\mathcal{P}_{\text{ref}}}{d\lambda}\right)_{\text{peak}}} \frac{\mathcal{P}_{\text{AIB}}}{F_{\text{AIB}}}. \quad (4)$$

Table 1. Detection limits estimated for three test bands of neutral naphthalene, along with the parameters used to derive them. Two entries are listed for the perpendicular band at 58.56 μm , corresponding to the resolving power of LWS with and without the Fabry–Perot filter.

Band (μm)	S	$\frac{dF_{\text{cont}}}{d\lambda}$ $\left(\frac{\text{W}}{\text{cm}^2 \mu\text{m}}\right)$	R	$\left(\frac{d\mathcal{P}_{\text{ref}}}{d\lambda}\right)_{\text{peak}}$ $\left(\frac{\text{W}}{\text{sr } \mu\text{m}}\right)$	$\eta_{3.3}$	$\eta_{12.7}$
15.82	25	$4.6 \cdot 10^{-16}$	—	$7.3 \cdot 10^{-28}$	> 1	> 1
27.74	45	$1.5 \cdot 10^{-16}$	—	$1.5 \cdot 10^{-28}$	> 1	> 1
58.56	35	$1.5 \cdot 10^{-18}$	h	$5.4 \cdot 10^{-29}$ $6.5 \cdot 10^{-29}$	0.52 0.44	0.42 0.34

This derivation is completely general, despite the fact that we wrote it for neutral naphthalene and applies to any specific band of any specific PAH. We can now put the numbers for the three bands we studied in detail for neutral naphthalene. Upon examination of the previously calculated spectra, the strongest emission bands of neutral naphthalene in the RR are the in-plane C–H stretch at $\sim 3.3 \mu\text{m}$ and the out-of-plane C–H bend at $\sim 12.7 \mu\text{m}$; the fraction of the total IR emission of neutral naphthalene in such bands is calculated to be respectively 58.9% and 26.5%. From observations of the RR available from the online ISO database, their integrated band intensities amount to $F_{3.3} = 7.35 \cdot 10^{-17} \text{ W cm}^{-2}$ and $F_{12.7} = 3.51 \cdot 10^{-17} \text{ W cm}^{-2}$. From our model we have, for neutral naphthalene, $\mathcal{P}_{3.3} = 2.42 \cdot 10^{-26} \text{ W sr}^{-1}$ and $\mathcal{P}_{12.7} = 9.08 \cdot 10^{-27} \text{ W sr}^{-1}$, while the values of S and $\frac{dF_{\text{cont}}}{d\lambda}$ estimated from ISO archive data and those of $\left(\frac{d\mathcal{P}_{\text{ref}}}{d\lambda}\right)_{\text{peak}}$ calculated by our model (see Figs. 3 to 5) are listed in Table 1, along with the resulting detection limits at $\sim 2\sigma$ level. Since η_{AIB} was defined as the fraction of the flux observed in a given AIB which is produced by this specific molecule, a detection limit $\eta_{\text{AIB}} > 1$ means that the corresponding band (1st column in the table) is undetectable with the achieved S/N ratio. The perpendicular band, with its prominent central Q branch, is a much more sensitive (about two orders of magnitude) probe for neutral naphthalene, yielding the lowest detection limit of $\eta \sim 0.4$ for both reference AIBs considered. Resolving power helps a little, since separating single hot bands yields a higher peak flux in the strongest ones.

None of these bands are detected in ISO archive data, therefore we here obtained a direct observational upper limit on η for neutral naphthalene in the RR.

Turning to anthracene, its strongest emission bands in the RR are again the in-plane C–H stretch at $\sim 3.3 \mu\text{m}$ and the out-of-plane C–H bend at $\sim 11.3 \mu\text{m}$; the fraction of the total IR emission of neutral anthracene in such bands is calculated to be respectively 37.5% and 17.2%. The integrated intensities in the former of these bands observed in the RR was given above, the one of the $\sim 11.3 \mu\text{m}$ band

Table 2. Detection limits estimated for three test bands of neutral anthracene, along with the parameters used to derive them. Two entries are listed for the perpendicular band at 26.35 μm , corresponding to the resolving power of SWS with and without the Fabry–Perot filter.

Band	S	$\frac{dF_{\text{cont}}}{d\lambda}$	R	$\left(\frac{d\mathcal{P}_{\text{ref}}}{d\lambda}\right)_{\text{peak}}$	$\eta_{3.3}$	$\eta_{11.3}$
(μm)		$\left(\frac{\text{W}}{\text{cm}^2 \mu\text{m}}\right)$		$\left(\frac{\text{W}}{\text{sr } \mu\text{m}}\right)$		
21.26	50	$3.1 \cdot 10^{-16}$	—	$4.2 \cdot 10^{-27}$	> 1	0.44
26.35	90	$1.9 \cdot 10^{-16}$	l	$5.1 \cdot 10^{-28}$	> 1	> 1
43.68	75	$4.9 \cdot 10^{-17}$	h	$7.2 \cdot 10^{-28}$	> 1	0.86
110.23	25	$1.5 \cdot 10^{-18}$	l	$6.0 \cdot 10^{-29}$	> 1	0.33
			h	$7.2 \cdot 10^{-29}$	> 1	0.27

is measured to be $F_{11.3} = 1.39 \cdot 10^{-16} \text{ W cm}^{-2}$. Our model yields, for neutral anthracene, $\mathcal{P}_{3.3} = 4.7 \cdot 10^{-26} \text{ W sr}^{-1}$ and $\mathcal{P}_{11.3} = 2.15 \cdot 10^{-26} \text{ W sr}^{-1}$, while the values of S and $\frac{dF_{\text{cont}}}{d\lambda}$ estimated from ISO archive data and those of $\left(\frac{d\mathcal{P}_{\text{ref}}}{d\lambda}\right)_{\text{peak}}$ calculated by our model (see Figs. 6 to 9) are listed in Table 2, along with the resulting detection limits at $\sim 2\sigma$ level. Classical AIBs are not the only observable quantity against which ratios, and consequently η values, can be computed. Neutral anthracene, phenanthrene and pyrene were proposed as possible carriers of the Blue Luminescence (BL, Vijh et al. 2004, 2005), a fluorescence phenomenon observed in the Red Rectangle and, subsequently, in several other astronomical sources. In a previous work, we demonstrated that phenanthrene and pyrene could be ruled out based on the failure to detect their predicted IR emission spectra (Mulas et al. 2006a). Anthracene remained, of the three, the only candidate compatible with available ISO observations of the Red Rectangle. The strongest constraint appeared to be the undetected longest wavelength band at $\sim 110 \mu\text{m}$, which however contained a degree of uncertainty due to the unknown band profile. We here reproduce the comparison of the calculated band with available observations *including* the detailed modelling of band profile. This is shown in Fig. 10. The line of reasoning leading to Eq. (4) can be identically retraced substituting the integrated BL flux in the place of the integrated flux in a classical AIB (see Mulas et al. 2006a, for a detailed derivation). This yields $\eta_{\text{BL}} > 1$ for anthracene, i. e. it confirms that this band is undetectable with the available ISO database observations. It is however apparent (see Fig. 10) that this band is expected to be just slightly below the detection limit, and an increase in S/N of a factor of ~ 5 ought to reveal it, if anthracene indeed produces the observed BL.

4. Discussion and conclusions

The upper limits we derived are on the relative contribution of specific molecules to well defined classical AIBs, specifically

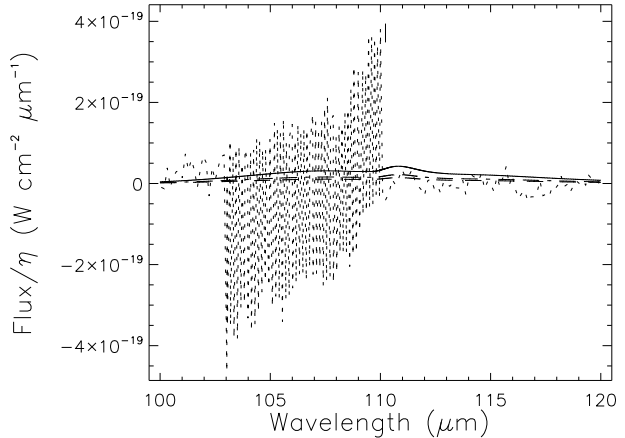


Fig. 10. Comparison between the estimated IR emission spectrum of anthracene ($\text{C}_{14}\text{H}_{10}$) and an ISO spectrum of the RR in the wavelength range $100\text{--}120 \mu\text{m}$. Calculated spectra, under different assumptions (see Mulas et al. 2006a, for details) are drawn in dashed, dash-dotted, and continuous lines; the continuum-subtracted ISO spectrum is shown as a dotted line. The central position of the fundamental of the expected anthracene band is marked by a tick, which shows the effect of anharmonic shifts.

at ~ 3.3 , ~ 11.3 and $\sim 12.7 \mu\text{m}$. They can be easily converted into absolute abundance limits, but this implies an assumption on their spatial distribution in the observed source and on the detailed assumed scaling of RF intensity. The terms depending on such assumptions cancel when using ratios of bands, making them more robust.

Despite obtaining very similar numerical values for the upper limits on $\eta_{3.3}$ and $\eta_{12.7}$ for naphthalene, their relevance is different. The $\sim 3.3 \mu\text{m}$ band is produced efficiently by small neutral molecules; the intensity of this band is suppressed in cations and rapidly decays with molecular size, as shown by Fig. 11. This implies that the PAHs significantly contributing to the $\sim 3.3 \mu\text{m}$ band are a small subset of the whole population, namely only the small ones. The number of different species in this subset is accordingly very much smaller, thus $< 40\%$ of the small PAHs (i. e. $\eta_{3.3}$) is a much stronger constraint than $< 40\%$ of all PAHs. This trend is much weaker for the flux fraction in the band at $\sim 12.7 \mu\text{m}$, as shown by Fig. 12. This is a consequence of the well-known variation in the position of the out-of-plane C–H bend depending on specific molecular parameters (e. g. *solo*, *duo*, *trio* modes etc.), hence chemical diversity produces a large scatter which dominates over size effects. This means that the band at $\sim 12.7 \mu\text{m}$ is not produced preferentially by a subset of PAHs defined by size, but instead by structure.

As to anthracene, we obtained rather weak constraints for $\eta_{3.3}$, somewhat stronger constraints on $\eta_{11.3}$. However, Fig. 13 shows that larger molecules can be expected to contribute a considerable fraction of the flux emitted in this band, which means that $\sim 40\%$ is not such a stringent limit for $\eta_{11.3}$. As for

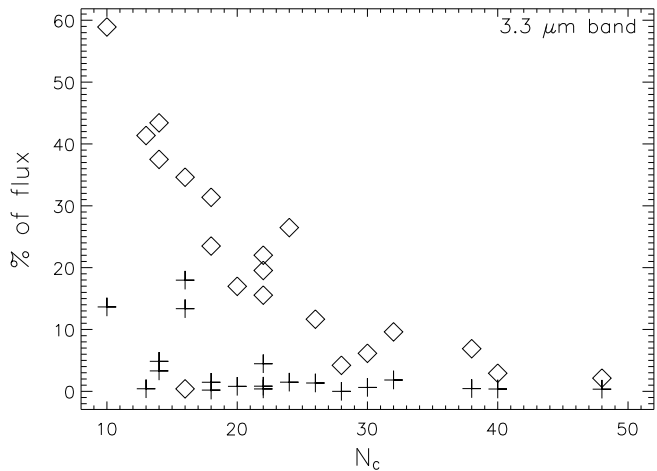


Fig. 11. Percentage of total IR flux emitted in the in-plane C–H stretch near $\sim 3.3 \mu\text{m}$, as computed by our model for the sample of molecules in Mulas et al. (2006b), as a function of molecular size. Neutral species are represented by diamonds, cations by crosses. For each molecule, we here considered all bands in the range 3.2 to $3.37 \mu\text{m}$, which corresponds to the observed width of the $3.3 \mu\text{m}$ band in the RR.

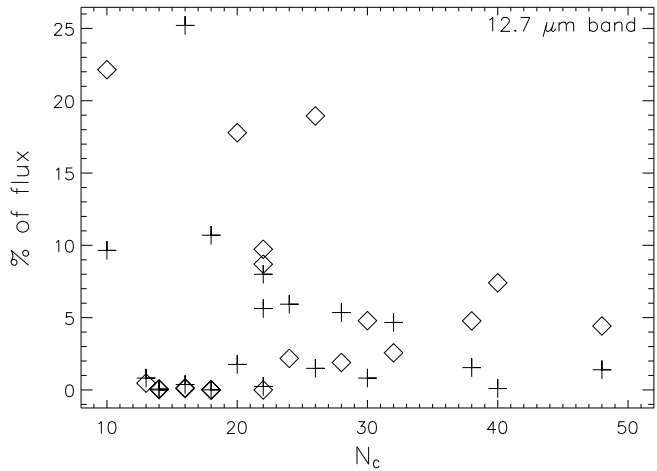


Fig. 12. Same as Fig. 11 for the out-of-plane C–H bend at $\sim 12.7 \mu\text{m}$. For each molecule, we here considered all bands in the range 12.3 to $13.1 \mu\text{m}$, which corresponds to the observed width of the $12.7 \mu\text{m}$ band in the RR.

the band at $\sim 12.7 \mu\text{m}$, the band at $\sim 11.3 \mu\text{m}$ is produced preferentially by a subset of molecules defined primarily by structure, more than by size.

While we applied our procedure to neutral naphthalene and anthracene, it can be generalised to any PAH for which our model is applicable and to any astronomical source for which observations of classical AIBs (or some other suitable tracer of PAHs) are available. As already mentioned, *all* PAHs have butterfly IR-active modes, which usually are the lowest frequency modes of each molecule and give rise to perpendicular bands (Mulas et al. 2006b). The lowest frequency vibrational modes

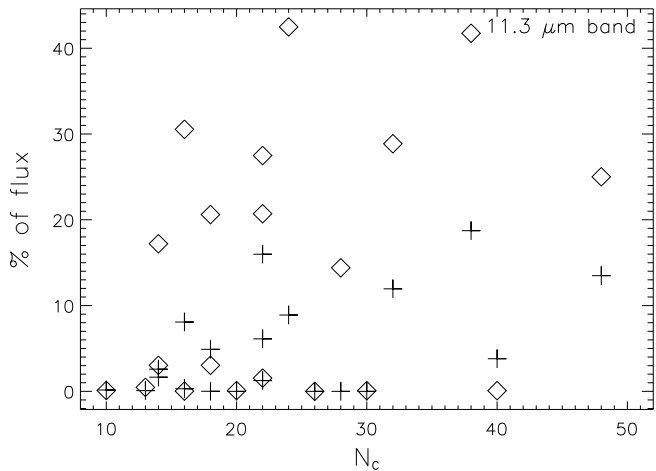


Fig. 13. Same as Fig. 11 for the out-of-plane C–H bend at $\sim 11.3 \mu\text{m}$. For each molecule, we here considered all bands in the range 10.9 to $11.7 \mu\text{m}$, which corresponds to the observed width of the $11.3 \mu\text{m}$ band in the RR.

are almost always well separated in energy (except for highly symmetric molecules), meaning that strong Coriolis perturbations are not likely to occur for them and they ought to display Q branches which can be very sharp, since the effective momenta of inertia can be very close between the upper and lower states of the transition. In turn, according to the present calculations these Q branches ought to contain $\sim 20\%$ of the total flux in the band, the distribution among fundamental and hot bands depending on the detailed statistics of the process and, essentially, on the vibrational modes which are left in an excited state upon decoupling. The spacing between the fundamental and various hot bands depends critically on the anharmonic vibrational constants χ_{ij} , which vary with the specific molecule and band considered. If a perpendicular band is emitted preferentially when the molecule has a very low excitation energy, then relatively few hot bands will contribute to it, their Q branches remaining well resolved and sharp, and the P and R branches blending and being somewhat blurred as a result. The same will happen if a few χ_{ij} are much larger than the others, producing a well-defined sequence of sharp Q branches.

We here modelled in detail the profiles of one perpendicular band of naphthalene and three of anthracene. Among them, three display sharp Q branches (Figs. 5, 7 and 9), in which fundamental and hot bands can be separated with adequate resolving power, the other one (Fig. 6) is red shaded to the point of partially washing out its structure. In this very limited sample, therefore, most perpendicular bands possess a combination of molecular parameters which yields the maximum spectral contrast. On a large sample of molecules, it can be reasonably expected that this will happen for some intense bands, producing the most favorable conditions for their detection.

In general, the average rotational energy of the molecule is expected to scale roughly with the average energy of the vibrational photons emitted (see e. g. Rouan et al. 1997), which implies that larger molecules ought to have a lower rotational energy which, together with decreasing rotational constants,

in turn translates to narrower rotational profiles and better detectability.

The mixture of PAHs in space probably contains a wide variety of different molecules, in principle in many different hydrogenation and ionisation states. However, Le Page et al. (2001, 2003) showed that in any given environment the population of a given PAH is expected to be dominated by one or two ionisation and hydrogenation states, essentially depending on its size and physical conditions. Furthermore, chemical selection effects will favour the most stable species over the others, so that at least *some* species may be abundant enough to exceed their detection limit on *some* η_{AIB} (or some other PAH tracer). Moreover, such a detection limit will be pushed one or two orders of magnitude lower by the much higher sensitivity of the instruments on board the forthcoming Herschel Space Observatory and by the much reduced dust continuum emission at longer wavelengths.

A systematic study of PAH band profiles and IR flux ratios is necessary to select the most promising diagnostics and species for identification. The search for single, specific PAHs in the far-IR is a challenging, but promising task.

Acknowledgements. G. Mallocci acknowledges the “Ministère de la Recherche” and G. Mulas the CNRS for the financial support during their stay at CESR in Toulouse. We thank Aude Simon for helping us to effectively use the GAUSSIAN03 package. Part of the calculations used here were performed using CINECA and CALMIP supercomputing facilities. This work was supported by the European Research Training Network “Molecular Universe” (MRTN-CT-2004-512302).

References

Allamandola, L. J., Tielens, A. G. G. M., & Barker, J. R. 1985, ApJ, 290, L25
 Allamandola, L. J., Tielens, G. G. M., & Barker, J. R. 1989, ApJS, 71, 733
 Barone, V. 2004, J. Chem. Phys., 120, 3059
 Barone, V. 2005, J. Chem. Phys., 122, 014108
 Barone, V. & Minichino, C. 1995, J. Mol. Struct. (Theochem), 330, 365
 Becke, A. D. 1993, J. Chem. Phys., 98, 5648
 Bregman, J. D., Rank, D., Temi, P., Hudgins, D., & Kay, L. 1993, ApJ, 411, 794
 Clabo, D. A., Allen, W. D., Remington, R. B., Yamaguchi, G., & Schaefer III, H. F. 1988, Chem. Phys., 123, 187
 Frisch, M. J., Trucks, G. W., Schlegel, H. B., et al. 2003, Gaussian 03, Revision B.05, Gaussian Inc., Pittsburgh PA, 2003
 Frish, M. J., Pople, J. A., & Binkley, J. S. 1984, J. Chem. Phys., 80, 3265
 Herzberg, G. 1991a, Electronic Spectra and Electronic Structure of Polyatomic Molecules, Vol. 3 of Molecular Spectra and Molecular Structure (Krieger Drive, Malabar, Florida: Krieger Publishing Company)
 Herzberg, G. 1991b, Infrared and Raman Spectra of Polyatomic Molecules, Vol. 2 of Molecular Spectra and Molecular Structure (Krieger Drive, Malabar, Florida: Krieger Publishing Company)

Joblin, C., Toublanc, D., Boissel, P., & Tielens, A. G. G. M. 2002, Molecular Physics, 100, 3595
 Langhoff, S. R. 1996, J. Phys. Chem., 100, 2819
 Le Page, V., Snow, T. P., & Bierbaum, V. M. 2001, ApJS, 132, 233
 Le Page, V., Snow, T. P., & Bierbaum, V. M. 2003, ApJ, 584, 316
 Léger, A., d'Hendecourt, L., & Defourneau, D. 1989, A&A, 216, 148
 Léger, A. & Puget, J. L. 1984, A&A, 137, L5
 Mallocci, G., Mulas, G., & Benvenuti, P. 2003, A&A, 410, 623
 Men'shchikov, A. B., Schertl, D., Tuthill, P. G., Weigelt, G., & Yungelson, L. R. 2002, A&A, 393, 867
 Mulas, G. 1998, A&A, 338, 243
 Mulas, G., Mallocci, G., & Benvenuti, P. 2003, A&A, 410, 639
 Mulas, G., Mallocci, G., Joblin, C., & Toublanc, D. 2006a, A&A, 446, 537
 Mulas, G., Mallocci, G., Joblin, C., & Toublanc, D. 2006b, submitted to A&A
 Pirali, O., Vervloet, M., Mulas, G., Mallocci, G., & Joblin, C. 2006, in preparation
 Rouan, D., Léger, A., & Le Coupanec, P. 1997, A&A, 324, 661
 Salama, F. 1999, in Solid Interstellar Matter: The ISO Revolution, ed. L. d'Hendecourt, C. Joblin, & A. Jones, (Les Ulis: EDP Sciences), 65
 Stephens, P. J., Devlin, F. J., & Chabalowski C. F., Frisch, M. 1994, J. Phys. Chem., 98, 11623
 Straatsma, T. P., Apra, E., Windus, T. L., et al. 2003, NWChem, A Computational Chemistry Package for Parallel Computers, Version 4.5
 Vlijh, U. P., Witt, A. N., & Gordon, K. D. 2004, ApJ, 606, L65
 Vlijh, U. P., Witt, A. N., & Gordon, K. D. 2005, ApJ, 619, 368
 Zhang, K., Guo, B., Colarusso, P., & Bernath, P. F. 1996, Science, 274, 582

Appendix A: Computed molecular parameters from the vibro-rotational analyses

In the following we report some of the molecular parameters obtained in the vibro-rotational analyses performed for neutral naphthalene and neutral anthracene at the B3LYP/4-31G level of theory. Tables A.1 and A.3 report, respectively, the vibrational anharmonic constants χ_{ij} for the three bands of neutral naphthalene and the four bands of neutral anthracene considered. The changes of the effective rotational constants as a function of vibrational state are reported in Tables A.2 for naphthalene and A.4 for anthracene. For consistency, we list in the tables the frequencies we previously obtained (Mulas et al. 2006b) using the NWChem package (Straatsma et al. 2003) at the same level of theory. Frequencies obtained by GAUSSIAN03 (Frisch et al. 2003) are coincident within numerical errors. We give more significant digits than the actually expected accuracy to distinguish very close vibrational modes.

Table A.1. Anharmonic constants χ_{ij} (expressed in cm^{-1}) obtained at the B3LYP/4–31G level for the three vibrational modes of naphthalene neutral for which we modelled the detailed rotational structure.

Fundamental (μm)	15.820 μm	27.731 μm (cm^{-1})	58.196 μm
3.249	-0.126	0.004	0.035
3.250	-0.123	-0.018	0.039
3.265	-0.198	0.083	0.012
3.267	-0.198	0.032	0.018
3.280	-0.156	0.217	-0.014
3.284	-0.130	0.175	-0.026
3.286	-0.198	0.131	0.002
3.288	-0.178	0.123	-0.008
6.179	-1.360	-1.051	-0.449
6.278	-0.406	-1.057	-0.306
6.407	-1.347	-0.198	-0.239
6.632	-1.163	-0.519	-0.309
6.836	-0.735	0.180	-0.077
6.842	-0.659	-0.563	-0.240
7.146	-0.486	0.061	-0.055
7.335	-1.522	-0.039	-0.332
7.364	-1.765	0.820	-0.110
7.875	-0.630	0.704	-0.110
7.961	-0.305	0.038	-0.065
8.273	-0.406	-1.356	-0.327
8.527	0.011	1.270	0.207
8.551	-0.344	-0.482	-0.010
8.658	0.044	0.165	-0.055
8.838	-0.382	0.441	-0.229
9.812	0.082	0.824	-0.034
9.906	0.089	0.099	-0.066
10.065	-0.189	-0.052	-0.021
10.141	-0.140	-0.115	-0.126
10.389	-0.089	-0.004	-0.294
10.601	-0.024	-0.068	-0.157
10.638	-1.126	0.150	-0.083
11.294	-0.221	-0.088	-0.457
11.937	-0.325	-0.089	-0.245
12.545	-0.088	-1.264	0.292
12.691	-0.064	-0.176	-0.155
12.957	-0.335	0.050	-0.190
13.312	0.859	-0.252	-0.077
13.937	0.046	0.087	-0.093
15.825	0.105	-0.104	-0.200
15.895	-0.226	-0.221	-0.463
19.503	0.057	-0.095	0.339
19.536	0.050	0.254	0.807
20.878	0.237	0.226	-0.054
21.162	-0.225	-0.324	-0.349
25.745	0.259	-0.295	-0.579
27.737	-0.104	0.236	0.363
53.950	-0.113	-0.460	-0.230
58.565	-0.200	0.363	-0.258

Table A.2. The a_i , b_i and c_i constants (in units of 10^{-4} cm^{-1}) as obtained at the B3LYP/4–31G level for neutral naphthalene. These quantities express the change of the rotational constants as a function of the vibrational mode. For comparison, the rotational constants A, B and C in the vibrational ground state are 0.103289, 0.040779 and 0.029241 cm^{-1} , respectively.

Fundamental (μm)	a_i (10^{-4} cm^{-1})	b_i (10^{-4} cm^{-1})	c_i
3.249	0.346	0.080	0.065
3.250	0.347	0.077	0.063
3.265	0.320	0.087	0.068
3.267	0.323	0.081	0.064
3.280	0.325	0.096	0.073
3.284	0.323	0.093	0.070
3.286	0.313	0.087	0.069
3.288	0.313	0.088	0.068
6.179	0.800	0.519	0.136
6.278	0.471	0.387	0.187
6.407	1.061	0.307	0.478
6.632	0.661	0.241	0.303
6.836	0.410	0.055	-2.109
6.842	-0.124	0.302	2.421
7.146	-0.199	0.136	0.081
7.335	1.918	0.531	0.395
7.364	0.683	0.339	0.280
7.875	0.299	0.161	0.104
7.961	0.214	0.094	0.220
8.273	-0.055	0.458	0.324
8.527	-0.625	0.003	0.077
8.551	0.250	0.098	0.028
8.658	-0.199	0.049	0.069
8.838	-0.488	0.102	0.324
9.812	0.809	-0.042	0.144
9.906	0.782	0.009	0.112
10.065	0.916	0.163	0.022
10.141	0.954	0.153	0.017
10.389	0.448	0.192	0.012
10.601	-2.638	0.159	0.002
10.638	2.807	0.004	0.141
11.294	0.546	0.157	0.005
11.937	0.194	0.017	-0.001
12.545	-2.053	0.193	0.117
12.691	2.656	0.057	-0.013
12.957	0.333	0.085	-0.029
13.312	0.514	0.057	0.139
13.937	0.319	0.107	-0.020
15.825	-40.137	-0.023	0.113
15.895	40.437	0.062	-0.045
19.503	-0.220	-0.037	-11.605
19.536	-0.220	0.061	11.782
20.878	0.053	0.025	-0.097
21.162	0.692	-0.008	-0.104
25.745	0.733	-0.042	-0.113
27.737	-1.792	-0.050	0.069
53.950	0.339	0.146	-0.150
58.565	2.085	-0.262	-0.249

Table A.3. Same as Fig. A.1 for the four vibrational modes of neutral anthracene for which we modelled the detailed rotational structure.

Fund. (μm)	21.232 μm	26.336 μm	43.060 μm (cm^{-1})	109.937 μm	Fund. (μm)	21.232 μm	26.336 μm	43.060 μm (cm^{-1})	109.937 μm
3.249	-0.079	-0.063	-0.027	0.045	9.946	0.062	-0.100	0.121	-0.041
3.249	-0.078	-0.065	-0.030	0.044	10.102	-0.389	-0.628	-0.032	-0.037
3.263	-0.096	-0.033	-0.004	0.029	10.116	-0.275	-0.742	-0.035	-0.036
3.263	-0.095	-0.035	-0.007	0.030	10.407	-0.660	-0.563	-0.009	-0.055
3.282	-0.149	0.044	0.058	0.007	10.470	-0.372	-0.520	-0.008	-0.059
3.283	-0.128	0.039	0.042	0.005	10.875	-0.420	0.020	-0.284	0.007
3.284	-0.135	0.023	0.035	0.014	11.003	-1.283	-1.905	-0.057	-0.163
3.286	-0.110	0.011	0.018	0.017	11.005	-0.348	-0.140	-0.148	0.205
3.292	-0.317	0.085	0.086	-0.008	11.315	-2.030	-0.563	-0.161	-0.036
3.295	-0.299	0.087	0.081	-0.011	11.690	-0.356	-0.376	-0.030	-0.100
6.162	-0.331	-0.554	-0.338	-0.143	11.982	-1.000	-0.666	-0.035	-0.096
6.183	-0.703	-0.614	1.810	-0.184	12.563	-0.517	-0.324	0.328	0.008
6.329	-0.421	-0.520	-1.023	-0.177	13.043	-3.945	-0.560	0.021	0.197
6.486	-0.559	-0.572	-0.028	-0.119	13.173	-0.291	-3.714	0.032	0.039
6.514	-0.376	-0.471	0.081	-0.161	13.434	-0.667	0.317	0.023	-0.098
6.736	-0.137	-0.297	-0.128	-0.096	13.512	-0.712	-0.806	-0.017	-0.027
6.860	-0.295	0.048	-0.554	-0.126	13.709	-0.367	-0.668	0.031	0.035
6.864	-0.021	-0.365	0.243	-0.040	15.329	-0.554	-0.136	-0.012	-0.209
7.147	-0.144	0.118	-0.072	-0.031	15.706	0.187	0.120	0.016	-0.160
7.218	-0.192	-0.813	-0.453	-0.110	16.336	0.066	-0.027	-0.481	0.131
7.218	-0.829	-0.933	0.704	-0.098	17.109	-0.112	-0.470	-0.277	-0.088
7.434	-0.989	-0.699	-0.845	-0.140	18.710	-0.287	-0.037	-0.073	0.265
7.605	-0.008	1.095	0.019	-0.067	20.037	-0.060	-0.499	0.050	0.151
7.768	0.290	-0.460	0.512	-0.031	21.019	0.209	-0.171	0.016	-0.192
7.848	2.118	-0.500	-0.024	-0.087	21.263	0.040	-0.065	-0.030	-0.002
7.899	-0.355	-0.226	0.006	-0.135	25.448	-0.200	-0.338	0.664	-0.424
8.318	-0.272	-0.491	0.045	-0.002	25.625	0.109	-0.064	-0.244	0.915
8.473	-0.318	-0.152	0.056	-0.137	26.349	-0.065	0.171	-0.271	-0.181
8.553	-0.196	0.349	0.069	-0.060	37.412	-0.237	-0.220	-0.408	0.017
8.623	-0.535	2.072	-0.178	-0.076	43.009	-0.129	-0.554	-0.978	-0.281
8.668	-0.349	-0.198	-0.221	-0.037	43.681	-0.030	-0.271	0.024	-0.587
9.107	-0.588	-1.000	-1.709	-0.117	82.090	-0.261	-0.269	-0.828	-0.173
9.911	0.105	-0.118	0.200	-0.040	110.231	-0.002	-0.181	-0.587	-0.146

Table A.4. Same as Fig. A.2 for neutral anthracene. The rotational constants A, B and C in the vibrational ground state are 0.071063, 0.014959 and 0.012361 cm⁻¹, respectively.

Fund. (μm)	a _i	b _i (10 ⁻⁴ cm ⁻¹)	c _i	Fund. (μm)	a _i	b _i (10 ⁻⁴ cm ⁻¹)	c _i
3.249	0.166	0.014	0.014	9.946	0.433	-0.001	0.027
3.249	0.166	0.014	0.014	10.102	0.430	0.025	0.005
3.263	0.155	0.015	0.015	10.116	0.434	0.024	0.005
3.263	0.155	0.015	0.014	10.407	0.193	0.029	0.003
3.282	0.161	0.020	0.018	10.470	0.072	0.023	0.001
3.283	0.157	0.018	0.016	10.875	0.154	0.018	0.035
3.284	0.155	0.018	0.017	11.003	0.211	0.031	0.004
3.286	0.152	0.016	0.015	11.005	-0.323	0.009	0.024
3.292	0.176	0.029	0.024	11.315	0.401	0.016	0.000
3.295	0.172	0.029	0.024	11.690	0.199	0.026	0.002
6.162	0.296	0.106	0.069	11.982	0.101	0.024	0.001
6.183	0.375	0.147	0.084	12.563	0.261	0.052	0.059
6.329	0.206	0.122	0.082	13.043	0.141	0.013	-0.005
6.486	0.539	0.081	0.106	13.173	0.238	0.008	-0.002
6.514	0.356	0.086	0.087	13.434	0.223	-0.004	-0.010
6.736	0.276	0.055	0.063	13.512	0.313	0.016	0.024
6.860	-0.009	0.092	-0.239	13.709	0.092	0.014	-0.002
6.864	0.198	0.024	0.334	15.329	0.008	0.037	-0.033
7.147	-0.073	0.036	0.027	15.706	-1.289	-0.003	0.015
7.218	0.671	0.117	0.117	16.336	-0.177	0.011	0.090
7.218	0.784	0.089	0.079	17.109	1.376	-0.018	-0.015
7.434	0.409	0.136	0.096	18.710	-0.250	0.015	0.022
7.605	-0.010	0.095	0.087	20.037	0.424	-0.019	-0.028
7.768	0.111	0.028	0.000	21.019	0.194	-0.007	-0.023
7.848	0.082	0.052	0.062	21.263	0.013	-0.004	-0.023
7.899	0.283	0.136	0.142	25.448	-0.683	-0.002	-1.019
8.318	0.165	0.009	0.031	25.625	-0.012	0.020	1.062
8.473	-0.268	0.004	0.014	26.349	0.355	-0.023	-0.032
8.553	-0.180	0.035	0.037	37.412	0.261	-0.006	-0.034
8.623	0.328	0.071	-0.448	43.009	0.904	-0.060	-0.059
8.668	-0.162	0.017	0.565	43.681	-1.292	-0.026	0.009
9.107	-0.236	0.070	0.055	82.090	0.124	0.026	-0.042
9.911	0.391	0.002	0.030	110.231	1.647	-0.082	-0.091